Journal of Power Sources 196 (2011) 1599–1607

Contents lists available at ScienceDirect

Journal of Power Sources

journal homepage: www.elsevier.com/locate/jpowsour

A reference governor-based hierarchical control for failure mode power management of hybrid power systems for all-electric ships☆

Gayathri Seenumani[a,*], Huei Peng[a], Jing Sun[b]

[a] Department of Mechanical Engineering, The University of Michigan, Ann Arbor, MI 48109, United States
[b] Department of Naval Architecture and Marine Engineering, The University of Michigan, Ann Arbor, MI 48109, United States

ARTICLE INFO

Article history:
Received 20 June 2010
Accepted 14 July 2010
Available online 4 August 2010

Keywords:
All-electric ships
Hybrid power systems
Power management
Real-time optimization
Reference governor

ABSTRACT

This paper deals with the design of failure mode power management (PM) of hybrid power systems (HPS) during a shipboard power source failure, which is an important scenario that the all-electric ships (AES) targeting military applications have to deal with. The control objective is to manage the power flow from working power sources and battery to ensure survivability, namely, ensuring system safety and maximizing the load support. The on-demand nature of the problem due to unpredictable failure times makes real-time control a key requirement. The survivability mandates, along with large scale, nonlinear HPS dynamics and long warmup times of the backup power sources, make most of the existing control strategies ineffective to meet the real-time requirements. With the focus on achieving real-time computational efficiency, a novel hierarchical control approach using reference governor is proposed. A top level controller determines a sub-optimal power split between the battery and working source to meet the demand on the HPS and the local controllers govern the power demands for the individual power sources to enforce constraints. A case study of the proposed controller on a scaled HPS test-bed illustrates the real-time computational efficiency and improved HPS survivability.

1. Introduction

As the engineering communities are seeking more clean and efficient ways of power generation, hybrid power systems (HPS) are becoming increasingly popular, and have been pursued as solutions for both land-based and mobile applications. The shipboard integrated power system (IPS) [1,2] used in all-electric ship (AES) is a representative example of HPS and provides the motivating application for this work. The main components of a typical DC HPS, as shown in Fig. 1, include power sources, power converters, energy storage devices (ESD) and loads. The key feature of a HPS is that it involves multiple power sources that can augment each other in the power generation capability to boost the overall system efficiency and reduce environmental impact. For the HPS targeting the AES, we consider gas turbine/generator and fuel cell for the power sources [3] given their complementary efficiency and dynamic characteristics. For ESD we use battery that has substantial storage capacity. Even though the load shown in Fig. 1 represents the entire power demand on the HPS, these loads are further classified as critical and non-critical [4] for the AES.

Given the heterogenous nature of the HPS components, power management (PM) of HPS is necessary to manage the power from the battery and sources to meet load demands in a timely manner. Since the shipboard HPS targeting military applications are highly susceptible to damages, the design of PM system should also protect the power system from the effects of the failures. Typically backup power sources can be used to deal with the failures, but these sources take time to warm up during which the ability of the HPS to meet the onboard power demand could be greatly compromised. Hence in this paper, we consider the optimal control of shipboard HPS during a power source failure, with the goal of improving survivability. In this work we define survivability as the capability of power management system to sustain critical shipboard operations and recover normal functions while ensuring the safety of the HPS components.

For the HPS considered in this work, the control objective is to determine the power that can be safely demanded from the battery and the working power source (gas turbine or fuel cell) and achieve optimal performance in terms of power tracking and efficiency. The optimal control has to deal with the following problem characteristics

- *On-demand* survivability goals due driven by the unpredictable timing of component failure.

☆ This work is supported by ONR under the Award No. N00014-03-1-0983.
* Corresponding author. Tel.: +1 734 239 5614; fax: +1 518 387 5164.
E-mail addresses: gseenuma@umich.edu (G. Seenumani), hpeng@umich.edu (H. Peng), jingsun@umich.edu (J. Sun).

0378-7753/$ – see front matter © 2010 Elsevier B.V. All rights reserved.
doi:10.1016/j.jpowsour.2010.07.041

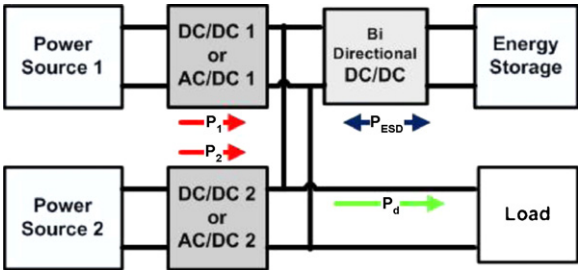

Fig. 1. Example of a hybrid power system.

- Long time horizon associated with warm-up periods of a backup power source.
- Difficulties in obtaining analytical models for HPS components.
- Active use of energy storage to support critical functions when the back-up source is warming up.

These characteristics require that the optimal control has to be executed in real-time without computational delay and enforce component safety all through the extended time horizon till the back-up source is warmed up. These two requirements make the optimal control problem challenging.

The existing work on the failure mode PM for shipboard power systems [5–11] mostly deals with network restoration through load shedding and does not consider non-critical load support as a performance attribute. This attribute is especially important to improve survivability where recovering the normal shipboard functions is necessary.

The problem under consideration has been treated as trajectory planning problem in the power management of commercial hybrid land vehicles. Existing literature ([12,14] and references there-in) for the power management of fuel cell-battery hybrid systems consider both horizon based and instantaneous optimization methods. These include dynamic programming (DP) [12], stochastic dynamic programming (SDP) [13] and equivalent fuel consumption minimization (ECMS) [14]. While the "curse of dimensionality" makes DP impractical for real-time control, the lack of a transition probability function makes SDP and ECMS based methods unsuitable to attain the control objective considered in this work.

Model predictive control (MPC) [15,16] is another popular approach proposed in literature for solving the optimal control problem, where a relatively short time horizon can be considered for the benefits of computational efficiency. A receding horizon control (RHC) approach can be adopted in order to deal with the extended horizons associated with power source warm up times. While MPC is suitable for real-time control, one key disadvantage is the difficulty in achieving a good tradeoff between real-time computational efficiency and guaranteeing long term safety which motivates the need to seek alternate approaches for power management during failures. Here, we define the real-time computational efficiency as the ability to solve the optimal control problem at a given sample rate.

In this paper, we propose a hierarchical optimal control strategy that utilizes the power demand profile information to enforce component safety in the long-term and support the non-critical loads as much as possible while maximizing the battery usage. The key merits of the proposed approach are the real-time efficiency and the experimental validation results on a scaled test-bed. To achieve real-time efficiency, we explore the nature of the failure mode problem where constraint enforcement (namely ensuring component safety) is the key consideration and hence recast the optimal control problem to treat safety and performance separately.

At the top level, we ignore the component dynamics and determine the sub-optimal power split between the battery and the working source to meet the HPS load demand. At the second level, we formulate the constraint enforcement problem using reference governor (RG), where the demand to the working source and energy storage is governed to ensure safety [17,18]. The RG approach is a natural formalism for constraint enforcement. It involves a one-dimensional search (hence is much simpler as compared to other RHC methods) and allows long horizon look ahead without compromising real-time performance. In order to account for the performance deterioration due to ignoring power source dynamics at the top level, we utilize the battery to improve the power tracking performance based on coordination between the working source and energy storage.

The paper is organized as follows: In Section 2, the optimal control problem for failure mode PM is formulated and the hierarchical controller is proposed. In Section 3, the HPS model is summarized. The proposed controller is applied to the HPS model and the real-time optimization results on an experimental test-bed are presented in Section 4, along with concluding remarks in Section 5.

2. Problem formulation and proposed hierarchical controller

In this section we formulate the optimal control problem and propose the hierarchical control strategy. We ignore the power converters and only consider the battery and power sources for HPS components, given the fact that the dynamics of the power converters (μs) are much faster as compared to the sources (ms). We consider the scenario of a power source failure with unpredictable failure time, even though the ideas used in the controller development can be extended to failure of other HPS components. We assume that a back-up source is added to the HPS at the instant the failure occurred and define the warmup period as the time from the instant of failure to the time when the back-up source is fully functional. Then, the problem is formulated to capture the following objectives during the warm-up period.

- Enforcing the battery and working power source physical constraints throughout the backup power source warming up period.
- Meeting the critical load demand all through the warmup period and support the non-critical loads as much as possible.

It must be noted that for the HPS considered in this work, the working power source can be either gas turbine or fuel cell. We first describe the power plants and the safety constraints before formulating the optimal control problem. The nomenclature adopted in the power management controller development is given in Table 1.

Without loss of generality, we denote $T_F = 0$ as the instant when one of the power source fails, at which an additional power source is brought on with a warm-up time represented by T_w discrete time steps, where $[0, T_w]$ is the warmup horizon. Let $f_S(x_S, u_S)$, $h_S(x_S, u_S)$ denote the working source (gas turbine or fuel cell) dynamics and

Table 1
Nomenclature used in PM controller design.

Variable	Description
x_S, u_S, P_S	Working source states, control inputs and power output (kW)
SOC, Q_B	Battery state of charge and capacity (Ah)
I_B	Current drawn from the battery (A)
V_B, P_B	Battery voltage (V) and power output (kW)

Script	Description
cr	Vital/critical load
d	Demand/reference variable
rg	Reference governor output
SS, *	Steady state and optimal variables

output function respectively. Then, the nonlinear HPS dynamics are described by

$$x_{S,k+1} = f_S(x_{S,k}, u_{S,k}) \tag{1}$$

$$\begin{aligned} SOC_{k+1} &= f_B(SOC_k, I_{B,k}) \\ P_{S,k} &= h_S(x_{S,k}, u_{S,k}) \\ P_{B,k} &= h_B(SOC_k, I_{B,k}) \end{aligned} \tag{2}$$

where $u_{S,k}$ is the fuel input to the working power source.

We consider two constraints that the control algorithm has to enforce during the warmup period:

1. Component Physical Constraints:
   - To prevent gas turbine compressor surge or fuel cell hydrogen starvation, depending on which power source fails (Φ_S), and ensure that the battery power and capacity are less than their corresponding maximum limits (P_B^{Max}, Q_B^{Max}). These constraints are given by,

$$\Phi_S(x_{S,k}, u_{S,k}) \le 0, \tag{3}$$

$$\Phi_B(SOC_k, I_{B,k}) \le 0, \tag{4}$$

     where $\Phi_B = [P_{B,k} - P_B^{Max},\ Q_{B,k} - Q_B^{Max}]^T$
   - To ensure that the control inputs are within the saturation limits given by

$$u_{S,k} \in [u^{Min}, u^{Max}]. \tag{5}$$

2. Critical demand constraint given by

$$-P_{S,k} - P_{B,k} \le -P_{cr,k}. \tag{6}$$

The cost function J captures the performance in terms of minimizing the power tracking error and working source fuel consumption over the warmup horizon and is given by

$$J = \sum_{k=0}^{T_w} u_{s,k} + \lambda(P_{d,k} - P_{S,k} - P_{B,k})^2$$

where $\lambda \gg 1$ is a penalty factor to achieve fast demand tracking. Then the optimal control problem formulation is given by

$$[I^*_{B,[0:T_w]}, u^*_{S,[0:T_w]}] = \arg\min_{I_{B,k}, u_{S,k}} J \tag{7}$$

subject to constraints (1)–(6) that need to be enforced over $[0, T_w]$.

Given the extended warmup horizon and the computational demand in solving the optimization problem (7), we have to consider a shorter prediction horizon of length $N (N \ll T_w)$ in order to use the MPC approach for real-time control. The optimal control inputs at every time instant $(u^*_{S,k}, I^*_{B,k})$ are then determined by solving the following problem

$$[I^*_{B,[k:k+N-1]}, u^*_{S,[k:k+N-1]}] = \arg\min_{I_{B,k}, u_{S,k}} \sum_{i=k}^{k+N-1} u_{S,i} + (P_{d,i} - P_{S,i} - P_{B,i})^2, \tag{8}$$

subject to constraints (1)–(6). Note that for the MPC formulation, the constraints are enforced over the prediction horizon, namely $[k, k+N-1]$, where k is any given time instant. To determine the optimal control inputs over the entire warmup period, the problem in (7) is solved repeatedly for every time instant $k \in [0,\ T_w]$ adopting the receding horizon approach.

Remark 1. The MPC problem in (8) is a nonlinear optimization problem whose computational effort depends on the dimension of the problem, namely the number of states (n), control inputs (m) and length of the optimization horizon (N). For most of the existing algorithms, the computational effort required to determine the optimal solution does not scale linearly with the addition of more HPS components. In addition, the choice of N plays a very important role as there exists a trade-off between reducing the computational effort and enforcing safety constraints. A short-sighted approach (*small N*) may significantly reduce the computational effort, but cannot guarantee successive feasibility[1] during the warmup period.

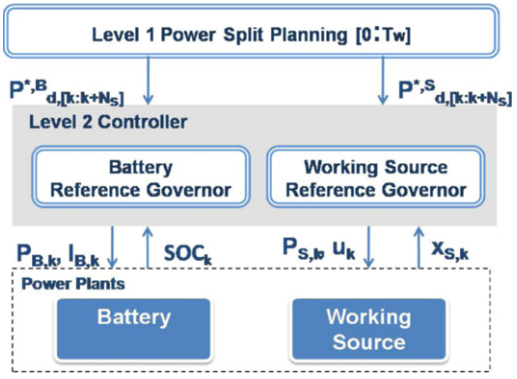

Fig. 2. Structure of the proposed hierarchical controller.

The issue raised in Remark 1, motivates us to seek alternate control approaches to solve the failure mode PM in (7), given the real-time control requirement.

2.1. Hierarchical RG-based control

Given the large scale nature of the problem, our goal is to simplify the problem (7) by leveraging the nature of the control required for failure mode operations. Here the primary function of the PM is to achieve safety enforcement during the entire the warmup period. Since the power tracking performance is secondary to the safety enforcement, the key idea used in the proposed controller is to decouple the power tracking from constraint enforcement and recast the optimization problem in (7) to treat the two requirements separately. This approach allows using simpler mechanisms targeting constraint enforcement (e.g reference governor). The following assumptions are made before proceeding to the controller development.

A1. Power can be drawn instantaneously from the battery pack subject to the capacity limits.

A2. For the HPS considered in this work, the fuel consumption for the power sources at steady state (W_f) is a quadratic function of the power demand (P), with $W_f = \Lambda(P)$.

A3. The power demand profile, namely the load demand on the HPS during the warmup period, is piecewise constant with κ step changes in load, where the time associated with each step and the constant value (after the step change) is denoted by K^j and P_d^j for $j \in [1, \kappa]$.

Under these assumptions, we propose a two level hierarchical controller (Fig. 2) to approximate the optimal solutions to the problem (7). At the top level, the battery and working source dynamics are ignored and a sub-optimal source battery power split is computed by solving a steady state optimization problem. Here we treat the battery storage mechanism and capacity as constraints. We consider the power split as sub-optimal solutions because even though the battery charge/discharge dynamics can be ignored using assumption A1, the power sources still have associated dynamics.

[1] Successive feasibility is defined as the existence of a feasible solution for the optimization problem at every iteration.

At the next level, we deal with the constraint enforcement over the warmup period using reference governor-based approach.

Remark 2. It must be noted that the fuel-power mapping function of the gas turbine or fuel cell need not be a quadratic function of the demanded power. However, in this work, we make assumption A2 based on curve-fitting the fuel cell and gas turbine individual fuel consumption versus the demanded power. The curve-fitting was done using the steady state fuel-power map of the power sources

Remark 3. Even though the RG can strictly enforce safety constraints, being an add-on mechanism it requires the reference inputs, namely the power demand to the working source and battery, to be pre-computed. Hence we need to solve the top level optimization problem in order to determine the sub-optimal battery, source power demand trajectories.

We delineate the proposed two level controller in the remainder of this section.

2.1.1. Level 1: quadratic programming for battery source power split planning

At this level, an approximate power split between the battery and the working source over the warmup period $[0 : T_w]$ is determined. The power split is computed by solving a steady state optimization problem, given the benefits of computational simplicity. Let α_B^j, α_S^j denote the battery, source power split parameter associated with each piecewise constant (See assumption A3) power level P_d^j and $P_{d,k}^S$, $P_{d,k}^B$ denote the power demand on the battery and source given by

$$P_{d,k}^S = \alpha_S^j P_d^j,\ k \in (K_j,\ K_{j+1}), \tag{9}$$

$$P_{d,k}^B = \alpha_B^j P_d^j. \tag{10}$$

The key idea is to formulate the cost function and the constraints in terms of the power split parameters because at this level our goal is to solve a steady state optimization problem. The cost function to achieve fast and efficient power tracking is defined as

$$J_1 = \sum_{k=0}^{T_w} \lambda (P_{d,k} - P_{d,k}^S - P_{d,k}^B)^2 + W_{f,k},$$

where $W_{f,k} = \Lambda(P_{d,k}^S)$ is the fuel consumption.

For the power sources, the input saturation constraints in (5) are specified in terms of the steady state minimum (P^{Min}) and maximum (P^{Max}) power corresponding to the working source fuel limits and is given by

$$P^{Min} \le P_{d,k}^S \le P^{Max}. \tag{11}$$

The battery constraints, namely the power and capacity limits are given by

$$P_{d,k}^B \le P_B^{Max}, \quad \forall k \in [0 : T_w], \tag{12}$$

$$\frac{1}{V_{dis}} \sum_{i=0}^{k} P_{d,i}^B \le Q_B^{Max}, \quad \forall k \in [0 : T_w], \tag{13}$$

where V_{dis} denote the battery discharge voltage.

The critical demand constraint in (6) is enforced using

$$-P_{d,k}^S - P_{d,k}^B \le -P_{cr,k} \tag{14}$$

If $\alpha_S = [\alpha_S^1, \ldots, \alpha_S^\kappa]$ and $\alpha_B = [\alpha_B^1, \ldots, \alpha_B^\kappa]$, the top leveoptimization problem is then given by

$$[\alpha_S^*, \alpha_B^*] = \arg\min_{\alpha_S, \alpha_B} J_1 \tag{15}$$

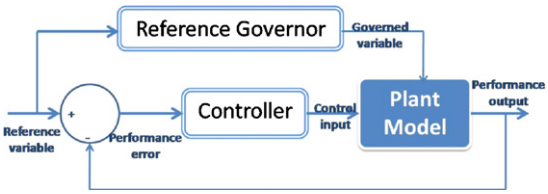

Fig. 3. Schematic of reference governor.

subject to constraints (11)–(14). The top level battery, source power demand trajectories denoted as $P_{d,[0:T_w]}^{*,B}$, $P_{d,[0:T_w]}^{*,S}$ is then computed using (9) and (10).

Remark 4. Under assumption A3, the optimization problem in (15) is a quadratic programming (*QP*) problem. The computational effort does not depend on the length of the planning horizon (N) or the number of states (n) and control inputs (m), and hence suitable for real-time implementation.

Remark 5. We consider the discharge voltage limit in (13) instead of the actual battery voltage (V_B) to compute the current drawn from the battery. This is done for two reasons: First, to formulate the capacity constraint as a linear constraint so that the top-level problem is a QP problem. Second, to ensure the nonlinear capacity constraint satisfaction (4), whenever the linear capacity constraint in (13) is enforced, where the nonlinear capacity constraint is given by

$$\frac{1}{V_{batt}} \sum_{i=0}^{k} P_{d,i}^B \le Q_B^{Max}, \quad \forall k \in [0 : T_w].$$

To see this, note that since $V_{dis} \le V_{batt}$, if $(1/V_{dis}) \sum_{i=0}^{k} P_{d,i}^B \le Q_B^{Max}$, this inequality implies that $(1/V_{batt}) \sum_{i=0}^{k} P_{d,i}^B \le Q_B^{Max}$. Even though this approach will result in a lower battery utilization as compared to the optimal solutions derived by solving (7), the benefits of the computational efficiency makes it attractive.

2.1.2. Level 2: reference governor for constraint enforcement

At this level, a reference governor is designed to track the power demand trajectories from level 1 ($P_d^{*,S}$ and $P_d^{*,B}$) as quickly as possible. This is an add-on mechanism (Fig. 3), where there is a designed nominal controller in the loop to regulate the performance variables. In this work, it is assumed that the nominal controllers are available and the focus will be directed to the reference governor design. Based on [18], the reference input, which is the power demand in this case, is modified at every time instant till the constraints (3)–(6) are satisfied and is determined as follows:

$$P_{rg,k}^S = P_{rg,k-1}^S + \beta_k^{*,S}(P_{d,k}^{*,S} - P_{rg,k-1}^S), \tag{16}$$

$$P_{rg,k}^B = P_{rg,k-1}^B + \beta_k^{*,B}(P_{d,k}^{*,B} - P_{rg,k-1}^B), \tag{17}$$

where $\beta_k^S, \beta_k^B \in [0, 1]$ can be viewed as nonlinear, time-varying filter parameters for the working source and battery, respectively.

In order to have the governed value, namely $P_{rg,k}^S, P_{rg,k}^B$, track the power demand, the RG maximizes the filter parameters (β_k^S, β_k^B) at every instant. The optimal filter parameters for the working source and battery are then determined as

$$\beta_k^{*,S} = \arg\max \beta_k^S \tag{18}$$

subject to constraints

$$\Phi_S(x_{S,i}, u_{S,i}) \le 0, \quad \forall i \in [k : k + N_s], \tag{19}$$

$$-P_{S,i} \le P_{B,i} - P_{cr,i}, \tag{20}$$

$$\beta_k^{*,B} = \arg\max \beta_k^B \tag{21}$$

subject to constraints

$$\Phi_B(SOC_i, I_{B,i}) \le 0, \quad \forall i \in [k : k+N_s], \tag{22}$$

$$-P_{B,i} \le P_{S,i} - P_{cr,i}, \tag{23}$$

where N_s is the simulation horizon inside which the constraints need to be enforced. This is done by simulating the model multiple times at each sampling instant to check the constraint feasibility given in (19), (20), (22) and (23). It must be noted that in the proposed two level controller, the optimal power split planning problem (15) is solved once at $k=0$, while (18) and (21) are solved at each instant k, with $x_{S,k}$, SOC_k being updated by the new state measurement for each new optimization run.

Remark 6. The optimization problems in (18) and (21) are 1D search problems as compared to the RHC approach where the dimension of the search space is mN. At each instant the optimization parameter (β_k) can be determined using bisectional search, where the *HPS* model is simulated for the simulation horizon ($[k : k+N_s]$). If constraint violation occurs then β is reduced and the simulation is re-initiated. If all the constraints are satisfied, then the value of β is increased to achieve better power tracking and the search is repeated till β converges.

Remark 7. The simulation horizon is chosen such that if the reference input is held constant after the time instant k and the constraints are satisfied over the time interval $[k{:}k+N_s]$, then they will be also satisfied over the interval for any $N_a > N_s$, which is typically the settling time of the system dynamics. To guarantee feasibility throughout the reconfiguration process, we choose a relatively large simulation horizon which is 3–5 times the system time constant. Even though a larger simulation horizon N_s implies increased model simulation time, since the search is over the optimization parameter space, this does not increase the optimization problem dimension and hence the computational effort. On the contrary, in the model predictive control approach, an increase in optimization horizon N will increase the dimension in search space and thus the computational effort.

Remark 8. In standard reference governor implementation, the input is held constant over the simulation horizon $[k : k+N_s]$. However, since the time-varying reference input is known during the entire warmup period for both the battery and the working power source, we utilize this information and hence consider the time varying reference input ($P^S_{d,[k:k+N_s]}$, $P^B_{d,[k:k+N_s]}$) in the implementation which is given as

$$P^S_{d,i} = \min(P^{S,*}_{d,i}, P^{S,*}_{d,k}), \quad \forall i \in [k, k+N_s], \tag{24}$$

$$P^B_{d,i} = \min(P^{B,*}_{d,i}, P^{B,*}_{d,k}). \tag{25}$$

The schematic of the reference governor implementation is given in Fig. 4.

2.1.3. Modifying reference input using coordination

Under assumption A1, the battery power output (P_B) will track the reference input ($P_d^{*,B}$) perfectly when $\beta_k^{*,B} = 1$. However, for the working source, even if the $\beta_k^{*,S} = 1$, there will be imperfect transient power tracking due to ignoring the source dynamics in the top-level optimization. Note that, since the battery can be used to support pulse loads (Assumption A1), we can utilize the battery to improve the transient power tracking. To do so, we use ideas from distributed model predictive control [19], where coordination between the battery and working power source is required. Here, the implementation requires communication from the working source to the battery at every instant regarding the steady state

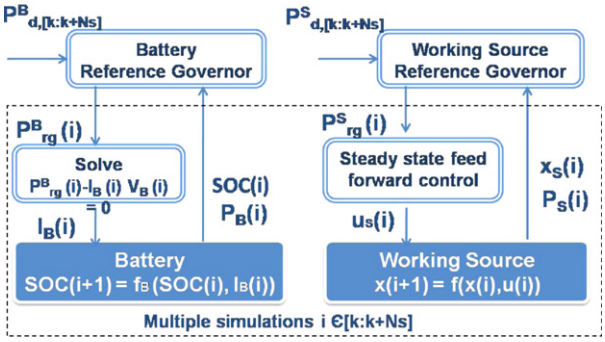

Fig. 4. Schematic of reference governor implementation.

control associated with the optimally governed reference trajectories. Then, at the next time instant, the reference input to the battery is modified based on the predicted working source power tracking performance.

Algorithm 1. Given $x_S(0)$, $SOC(0)$ and the power demand $P_{d,[0:T_w]}$, we propose the following algorithm to solve (7)

1. At $k=0$, determine optimal power split $P^{*,S}_{d,[0:T_w]}$ and $P^{*,B}_{d,[0:T_w]}$ by solving (15).
2. At each time instant k, using $P^{*,S}_{d,[k:k+N_s]}$, $P^{*,B}_{d,[k:k+N_s]}$,
   (a) Modify the reference input to the battery as $P^{*,B}_{d,[k:k+N_s]} + e^S$, where
   $$e^S = \begin{cases} 0_{1,N_s}, & k = T_f \\ P^{*,S}_{d,[k:k+N_s]} - P^C_{[k:k+N_s]}, & k > T_f \end{cases}$$
   where $P^C_{[k:k+N_s]}$ is the output trajectory associated with $u^C_{[k:k+N_s-1]}$ given by (26).
   (b) Compute the time varying $P^S_{d,[k:k+N_s]}$ and $P^B_{d,[k:k+N_s]}$ using (24) and (25).
   (c) Determine $P^S_{rg,[k:k+N_s]}$, $P^B_{rg,[k:k+N_s]}$ using (16) and (17).
   (d) Determine the feed-forward steady state control input $u_{S,[k:k+N_s]}$ associated with $P^S_{rg,[k:k+N_s]}$ and battery current $I_{B,[k:k+N_s]}$, given as
   $P^B_{rg,[k:k+N_s]} - I_{B,[k:k+N_s]} V_{B,[k:k+N_s]} = 0$,
   where the $V_{B,k}$ is the battery voltage.
   (e) Apply $u_{S,k}$ and $I_{B,k}$ (step 2(d)) as the approximation to the optimal solutions of (7).
   (f) Construct and transmit the coordination control sequence, to the battery which is given as

$$u^C_{[k+1:k+N_s+1]} = [u_{S,[k+1:k+N_s]},\ u^{SS}_{[k+N_s+1]}], \tag{26}$$

where $u^{SS}_{[k+N_s+1]}$ is the steady state control associated with the power demand to the working source $P^{*,S}_{d,[k+N_s+1]}$.

Remark 9. It should be noted that we denote the controller implementation as uncoordinated (w/o C) if the step 2(a) of Algorithm I is not implemented and with coordination (wC) if Algorithm I is exactly implemented.

3. Control-oriented HPS model

In this section, we develop an control-oriented dynamic model of the HPS in order to apply the algorithm proposed in Section 2. The HPS model consists of the component models, namely, battery, gas turbine and fuel cell whose dynamics are delineated below. For the case study presented in the sequel, we assume a gas turbine failure. Hence we will only summarize the fuel cell/reformer

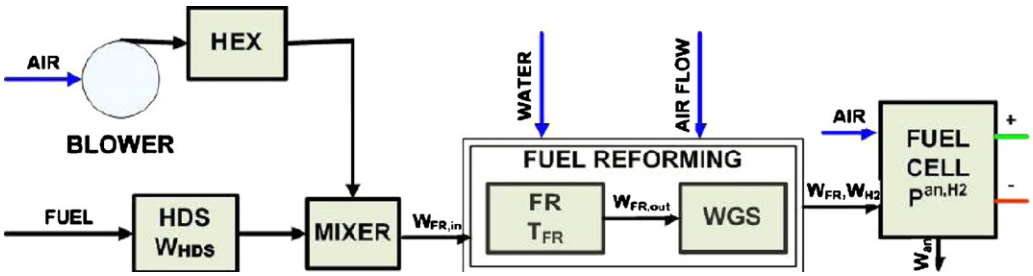

Fig. 5. Schematic of fuel cell and fuel reforming unit.

dynamics along with the battery model and further details on the HPS modeling can be found in [20].

3.1. Battery model

Even though many battery models have been proposed in [21], the resistance model is chosen for the sake of simplicity. The battery voltage V_B is given as

$$V_B = V_{oc}(SOC) - I_B R_B, \tag{27}$$

where $V_\propto$ is the open circuit cell voltage and R_{Batt} is the internal resistance of the battery. For this work, we use a *VL34P* Li-ion battery and using the data sheet the open circuit voltage is curve-fit as a sixth order polynomial of the battery capacity (Q_{Batt} in Amp-Hr). The internal resistance of the Li-Ion battery is assumed to be constant and is $R_{Batt} = 65\,\text{m}\Omega$ per module.

3.2. Fuel cell and reforming unit

We consider a Polymer Electrolyte Membrane (PEM) fuel cell along with a fuel processing system (FPS). The FPS+FC (Fig. 5) system consists of a hydro desulphurizer (HDS), heat exchanger (HEX), mixer (MIX), fuel reformer (FR) that converts the fuel flow to pure hydrogen, water gas shift reactor (WGS) for gas clean up and fuel cell anode dynamics. A detailed 10 state model of the FPS+FC system along with relevant assumptions has been developed in [22]. In this work, we summarize a reduced order model that captures the system dynamics as well as operating constraints such as fuel starvation. Based on the linear analysis of the 10 state model around different operating points, we found that the dominant modes corresponded to the FR temperature, HDS and the anode hydrogen partial pressure. Therefore, our reduced order model has three states. The inputs to the FPS+FC are fuel and air flow, while the stack current is considered as a disturbance. Since the stack current (I_{st}) is measured, the fuel and air flow are determined by a static feed-forward map to control the steady state fuel utilization (U_{H_2}) to 0.8 as given in [22]. The variables and parameters used in FC model are defined in Table 2 and the models of the dominant components are described as follows:

3.2.1. Hydro desulphurizer

The HDS is represented as a first order lag with a large time constant ($\tau_{HDS} = 5$ s) that reflects the slow dynamics of the linearized model given in [22], the other two slow dynamics being the FR temperature and the anode hydrogen partial pressure.

3.2.2. Fuel reformer

The FR model is developed in [22] and is summarized here. The temperature dynamics using energy balance is given by

$$\frac{dT_{FR}}{dt} = \frac{1}{m_{FR}c_{p,FR}}[N_{in}h_{in} - N_{out}h_{out}] \tag{28}$$

where the inlet flow consists of the fuel and air flow and the outlet flow includes the following species: CH_4, CO, CO_2, H_2, H_2O, and N_2.

Table 2
FC model nomenclature.

Variable	Description
$c_{p,FR}$	Constant ratio specific heat of FR material (kJ (kg K)$^{-1}$)
E	Open circuit fuel cell voltage
h_{in}, h_{out}	Specific enthalpy (J kg^{-1}) of inlet and outlet FR flows
m_{FR}	Mass inside the reformer unit (kg)
M_{an}, M_{H_2}	Molecular mass of anode material and hydrogen (kg mol^{-1})
n_c	Number of fuel cells in the stack
N_{in}, N_{out}	Molar flow rates in and out of the FR (mol s^{-1})
p_{an},$p_{H_2,an}$	Anode total and partial pressure (Pa)
R	Universal gas constant (J (K mol)$^{-1}$)
T_{FR}, T_{an}	FR and anode temperature (K)
v_{ohm}, v_{act}, v_{conc}	Ohmic, activation and concentration loss, respectively (V)
V_{an}	Anode volume (m^3)
$W_{FR,in}$	Total flow into the FR (kg s^{-1})
W_{FR,H_2}, $W_{FR,out}$	Hydrogen and total flow out of FR (kg s^{-1})
$W_{H_2,react}$	Reacted hydrogen inside anode (kg s^{-1})
$W_{H_2,an}$, W_{an}	Hydrogen and total anode exit flow (kg s^{-1})

3.2.3. Anode

The anode partial pressure dynamic using mass balance is given by

$$\frac{dp_{H_2,an}}{dt} = \frac{RT_{an}}{M_{H_2}V_{an}}(W_{FR,H_2} - \chi^{an}_{H_2}W_{an} - W_{H_2,react}),$$
$$\chi^{an}_{H_2} = \left(\frac{M_{H_2}}{M_{an}}\right)\left(\frac{p_{H_2,an}}{p_{an}}\right). \tag{29}$$

where W_{FR,H_2} is the hydrogen flow from the reformer, W_{an}, $W_{H_2,react}$ are the anode outlet flow and reacted hydrogen as given in [22]. The air supply is assumed to be instantaneous and the cathode pressure follows the anode pressure.

3.2.4. Stack voltage model

The stack voltage is a function of the fuel cell temperature and pressure and is given by $v_{st} = n_c(E - v_{act} - v_{ohm} - v_{conc})$. Further details of this model can be obtained from [22].

Table 3
HPS state and optimization parameters used in the case study.

Name	Value
Fuel cell states ($x_{s,0}$)	[0.23 mol s^{-1}, 90075.5 Pa, 963.2 K]^T
Battery SOC states (SOC_0)	1
Battery type	VL-39P Li-Ion (23 modules)
Critical demand	$P_{cr,k} \geq 1000$ kW
Starvation constraint	$0.04 - \frac{p_{H_2,an,k}}{p_{an,k}} \leq 0$
Maximum battery power (P_B^{Max})	95 kW per module
Maximum battery capacity (Q_B^{Max})	22 Ah per module
Sample time	$T_s = 0.05$ s
Failure instant	$T_f = 0$
Warmup period	$T_w = 5$ min

Fig. 6. Scaled test bed of HPS [23].

4. Case study

We consider a gas turbine failure for the case study and apply the proposed controller on the HPS model developed in the previous section. The demand on the HPS is represented as a hypothetical power profile (Fig. 7) that was chosen based on [2]. The case study parameters are shown in Table 3. Since we are emulating a gas turbine failure, the T_w is chosen to be $T_w = 5$ min, which corresponds to the warm-up times for ship-service gas turbines [2]. The main purpose of the case study is to illustrate the benefits of the controller in Algorithm 1. In particular two aspects are highlighted:

- Real-time computational efficiency of the proposed controller as compared to the MPC. We make the comparison using short and long constraint horizons in order to show that the proposed controller can have a longer simulation horizon without incurring polynomial increase in the computational effort. Therefore, the proposed method can be used to achieve long term constraint enforcement in real-time.
- Real-time performance improvement using the proposed controller as compared to the MPC method in terms of power tracking and fuel consumption.

We discuss these aspects mainly to show that even with the specific shipboard problem characteristics (described at the beginning

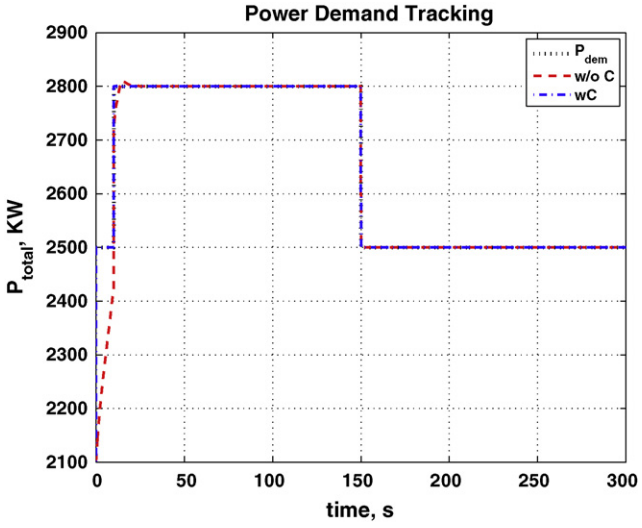

Fig. 7. Real-time power tracking with (wC) and without (w/o C) coordination.

Table 4
Comparison of RHC and RG methods for computational effort versus length of horizon.

Method	Horizon length	Off-line computation effort
RHC	$N = 40$	$T_{40}^{RHC} = 1783$ s
RHC	$N = 200$	$24.1\, T_{40}^{RHC}$
RG	$N_s = 40$	$T_{40}^{RG} = 6$ s
RG	$N_s = 200$	$1.2\, T_{40}^{RG}$

of this paper), the proposed controller can still enforce the safety constraint throughout the warmup period and support non-critical loads quickly in real-time. Even though safe backup strategies always exist, without the real-time efficiency, the survivability of the HPS will be compromised, either in terms of non-vital load support or the component safety.

The implementation of the two level hierarchical controller was done both off-line and in real-time where we used a Pentium® processor for the off-line and a dual core OpalRT® realtime target for online optimization. In the sequel, we first describe the experimental set-up and then the controller results.

4.1. Experimental setup

Fig. 6 shows the scaled test-bed for the hybrid power system, which includes the OpalRT® real-time simulator, two unidirectional and one bidirectional DC–DC full bridge convertors, DC power sources and loads. The two unidirectional DC/DC converters (marked as DC/DC1 and DC/DC2 in Fig. 6) are the Full Bridge Converter (FBC) while the bidirectional DC/DC converter (DC/DC 3) is the Dual Active Bridge Converter (DABC). The convertors used in the test-bed require 10 kHz modulation signals and have a bandwidth of 1 kHz and are much faster than the power sources considered in this work which have a bandwidth of about 10 Hz. The details on the hardware development for the DC–DC converters can be found in [23].

The two programmable power supplies are the *Sorensen*® SGA 100 A/100 V 10 kW AC/DC power supply. The output voltage of the programmable power can be controlled through an analog signal using OpalRT®, thereby making it a power source emulator. We use the 5.2 kW Chroma® 63204 10 A/100 A 125 V/500 V programmable DC loads to emulate the ship service load.

The OpalRT® simulator has the following functions: (1) running the controller and plant model in real-time; (2) commanding the DC power source to emulate the fuel cell; (3) generating the 10 kHz pulse width modulated (PWM) signals required for controlling the hardware-in-loop DC–DC convertors. For the case study, Target 1 runs at a sampling rate of 100 μs which is the base rate for the IPS model, while the other two targets run at 50 ms which is the sampling rate of the power generation module.

4.2. Optimization results and comparison

We consider two different lengths for the prediction (N) and simulation horizon (N_s) and solve the optimal control problem in (7) using the proposed controller and the RHC approach. The goal of this effort is to understand the tradeoff between computational effort and constraint enforcement, where a larger prediction horizon is required to ensure long term system safety.

Table 5
Real-time computational effort.

Method	Real-time computation effort	Off-line cost	Real-time cost
RHC $N = 40$	0.642 s	16.1	647
RG$N_s = 150$	0.0003 s	34.4	34.4

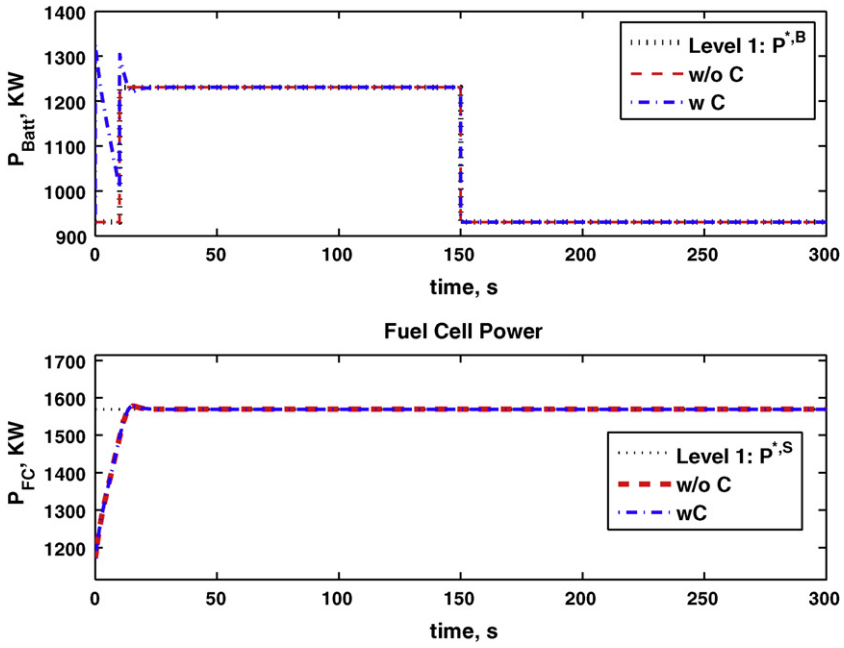

Fig. 8. FC and battery power split with (wC) and without (w/o C) coordination.

Table 4 shows the comparison of the offline computational effort of the RHC and RG methods as the optimization and simulation horizon is increased, respectively. We denote the computation effort associated with the shorter horizon for RHC ($N=40$) and RG ($N_s=40$) methods as T_{40}^{RHC}, T_{40}^{RG}. For this case study, we have $T_{40}^{RHC} = 1783$ s and $T_{40}^{RG} = 6$ s for a single optimization run at each sample instant. It can be seen that for the RHC based approach the increase is $O(N^2)$ (24.1 times) as compared to RG (1.2 times) which is in accordance with Remark 7.

The performance benefits of the proposed controller, due to its real-time computational efficiency, is illustrated in the sequel. Here, the performance is specified in terms of working source fuel consumption and power tracking error over the warmup period given as $\sum_{k=0}^{T_w} \lambda(P_{d,k} - P_{S,k} - P_{B,k})^2 + u_{S,k}$. The real-time computational effort along with the off-line and real-time performance is shown in Table 5. The off-line cost using the proposed control approach is sub-optimal as compared to the RHC approach (Column 3), which is due to ignoring the working source dynamics at

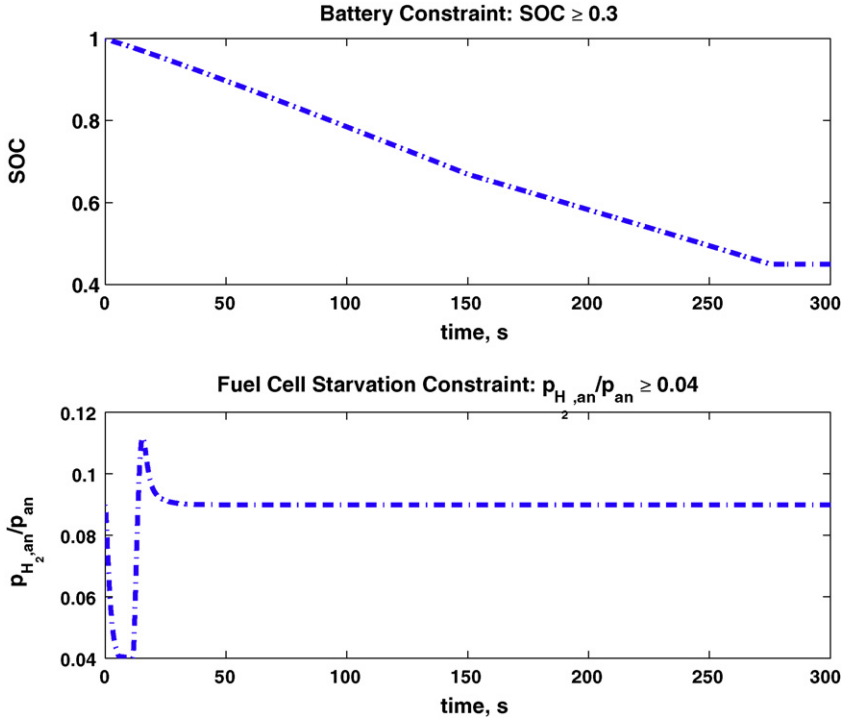

Fig. 9. Battery and fuel cell constraints for the case with coordination.

the top level controller. In real-time it takes 0.3 ms ($<T_s$) for the sub-optimal solutions to be available using the reference governor approach as compared to the 0.642 s ($>T_s$) when RHC method is implemented. Hence till the optimal solutions become available, we apply the control input at the previous instant to ensure constraint satisfaction which results in a performance loss in real-time using the MPC approach (Column 4).

Fig. 7 shows the real-time power tracking trajectories with (wC) and without (w/o C) using coordination (Remark 9). It can be seen that the demand tracking can be improved using coordination, where the battery can be utilized in order to compensate for the performance loss due to ignoring the fuel cell dynamics in the top-level optimization as shown in Fig. 8. The proposed controller enforces the fuel cell starvation constraint and the battery capacity constraint as shown Fig. 9. It can be seen that the battery state of charge constraint at the end of the warmup period is not active, which means that we are under utilizing the battery. Even though this may seem counter-intuitive at the onset, this is very much in accordance to Remark 6.

5. Conclusions

In this paper, we proposed a hierarchical optimal controller for failure mode power management of HPS for shipboard applications to sustain critical functions and recover normal operations during failures. The use of this approach is beneficial in ensuring HPS survivability due to the real-time computational efficiency. We have demonstrated using a case study that the proposed controller enforces the safety constraints in the long-term and also achieves better real-time performance as compared to model predictive control-based approach.

References

[1] T.J. McCoy, IEEE Power Engineering Society, 2002.
[2] N. Doerry, H. Robey, J. Amy, C. Petry, Naval Engineers Journal (1996).
[3] V. Tsourapas, J. Sun, A. Nickens, Proceedings of the 2006 Fuel Cell Seminar, 2006.
[4] C. Petry, J. Rumburg, Naval Engineers Journal (1993).
[5] K.L. Butler, N.D.R. Sarma, C. Whitcomb, H. Do Carmo, H. Zhang, IEEE Computer Applications in Power, 1998.
[6] S.K. Srivastava, K.L. Butler-Purry, N.D.R. Sarma, IEEE Computer Applications in Power, 2002.
[7] S. Srivastava, K.L. Butler-Purry, IEEE Proceedings of Generation, Transmission and Distribution, 2006.
[8] J.M. Solanki, N.N. Schulz, W. Gao, Proceedings of the 37th Annual North American Power Symposium, 2005.
[9] K. Huang, D.A. Cartes, S.K. Srivastava, IEEE Transactions on Systems, Man, and Cybernetics, 2007.
[10] M.E. Baran, N. Mahajan, IEEE Electric Ship Technologies Symposium, 2005.
[11] K. Davey, R. Longoria, W. Shutt, J. Carroll, K. Nagaraj, J. Park, T. Rosenwinkel, W. Wu, A. Arapostathis, Proceedings of the American Control Conference, 2007.
[12] K. Jeong, W. Lee, C. Kim, Journal of Power Sources (2005).
[13] M. Kim, H. Peng, Journal of Power Sources (2007).
[14] P. Rodatz, G. Paganelli, A. Sciarretta, L. Guzzella, Control Engineering Practice (2005).
[15] D.Q. Mayne, J.B. Rawlings, C.V. Rao, P.O.M. Scokaert, Automatica (2000).
[16] R. Ghaemi, J. Sun, I.V. Kolmonovsky, IEEE Conference on Decision and Control, 2007.
[17] E.G. Gilbert, I.V. Kolmonovsky, Automatica (2002).
[18] J. Sun, I.V. Kolmonovsky, IEEE Transactions on Control Systems Technology, 2005.
[19] W.B. Dunbar, R.M. Murray, Automatica (2006).
[20] G. Seenumani, Real-time Power Mangement of Hybrid Power Systems in All-Electric Ship Applications, Ph.D. Thesis, The University of Michigan, 2010.
[21] P.M. Gomadama, J.W. Weidner, R.A. Dougalb, R.E. Whitea, Journal of Power Sources (2002).
[22] J.T. Pukrushpan, A.G. Stefanopoulou, H. Peng, Control of Fuel Cell Power Systems, Springer, 2004.
[23] Y. Xie, J. Sun, C. Mi, J.S. Freudenberg, IEEE Vehicle Power and Propulsion Conference, 2009.